Electronic Supplementary Material (ESI) for Soft Matter.

Supplementary Information (SI)

Reinforced shape-tunable microwrinkles on a porous-film-embedded elastomer surface

Takuya Ohzono, Yuji Hirai, Kosuke Suzuki, Masatsugu Shimomura, and Nariya Uchida*

Contents:

Supplementary Information 1. Experimental details.

Sample preparation: The polymer porous film with "pillars" placed on a glass slide was fabricated (Fig. S1) from a self-organized honeycomb-patterned film,[24] which was prepared by casting a polystyrene (PSt) solution containing amphiphilic copolymers under humid conditions.[25] The periodicity (Λ) of the holes was ~11 μm. Polydimethylsiloxane (PDMS) was mixed using a two-part elastomer kit (Sylgard 184, Toray-Dow) with a 10:1 ratio (weight), before being cast onto the glass slide with the porous film having "pillars," covered to yield 12^2 mm^2 area and ~5 mm thickness, and cured overnight at 40 °C in an oven. PDMS was then peeled off and uniaxial compressive strain s (=0–0.20) was applied using a small vise to induce wrinkles. The angle (ϕ) between the strain axis and x-axis shown in Fig. S2 could depend on the domain of the hexagonal lattice of holes being observed. The applied strain here is defined as $s = |l - l_0|/l_0$, where l and l_0 are the actual and original length of the PDMS along the strain axis, respectively. As a reference system, PDMS coated with PSt was also prepared for being subjected to wrinkling and scratching tests by spin-coating a *N*-methylpyrrolidone (Sigma-Aldrich) solution of PSt (~4 wt%) onto a wettability-enhanced PDMS surface by a weak-plasma treatment (SEDE-P, Meiwa-Forsis). Upon uniaxial compression, the reference sample showed wrinkles with a wavelength of typically 25 μm.

Characterization methods: The sample was mainly characterized using an optical microscope (BX-51, Olympus) and an atomic force microscope (AFM5400, Agilent). For some other measurements, a scanning electron microscope (SEM, VE-8800, Keyence) and a laser microscope (VK-9710, Keyence) were used.

Scratching tests: Sample surfaces were scratched by a stainless needle with an apex radius of ~50 μm at a normal load of 100–200 mN and a sliding speed of ~1 mm s^{-1}.

Simulation: By extending a previous study,[1] we simply modeled the present system as an elastic membrabe with a two-dimensional modulus distribution corresponding to a hexagonal lattice and supported by a soft substrate. See Supporting Information 3 for details.

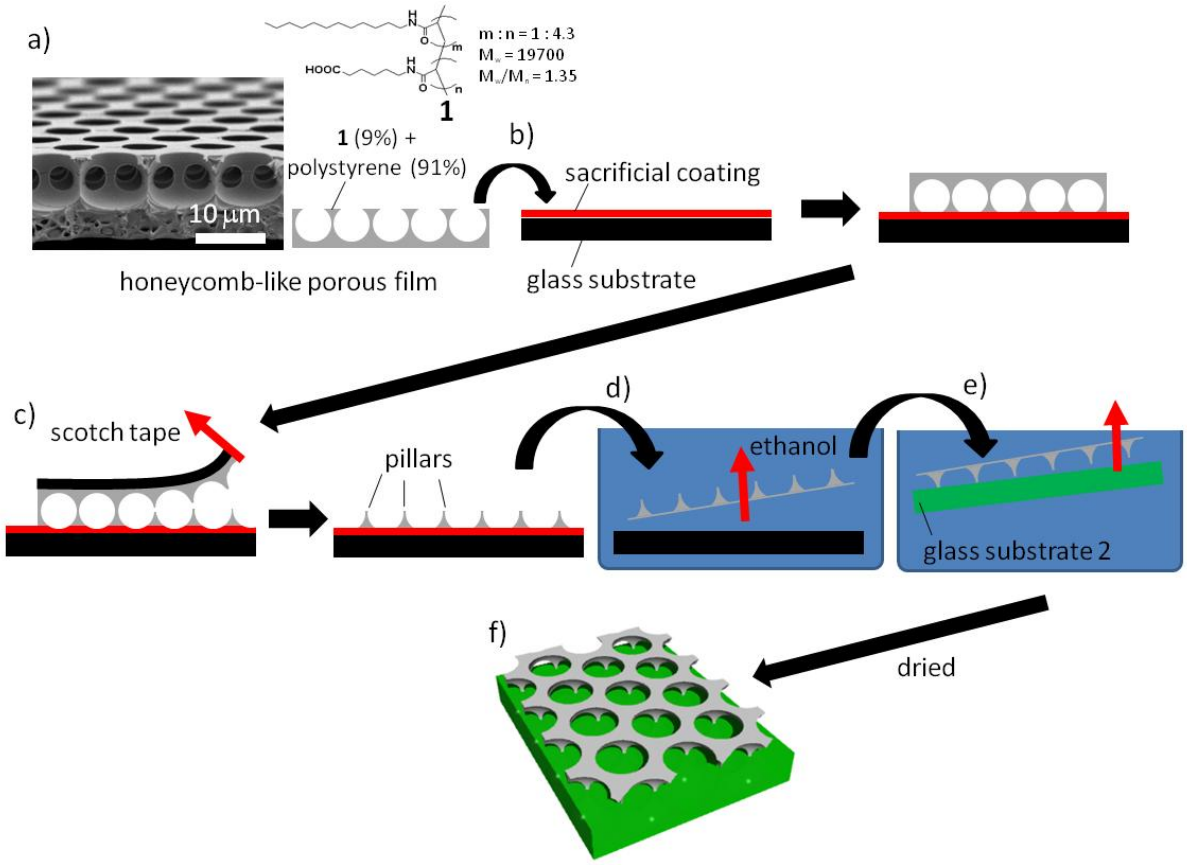

Figure S1. Preparation of a porous film with "pillars" placed on a glass slide. The porous film is prepared, through following procedures, from (a) a self-organized honeycomb-patterned film, which is fabricated by casting a polymer solution containing amphiphilic copolymers under humid conditions.[24,25] A hexagonally arranged water droplet array on the surface of the evaporating polymer solution works as a transient template for the porous film, through a well known "breathe figure" phenomenon. The film is composed of polystyrene (PSt, Mw: 280,000, Aldrich) and an amphiphilic polyacrylamide derivative (1, m:n = 4:1, synthesized through free-radical polymerization) (PSt:1 = 10:1). The film size is ~50^2 mm^2. The SEM image is also shown. Technical details are available in references.[24] Here, the periodicity, the in-plane hole-to-hole distance, of the porous film is Λ ~11 μm, which is adjusted by changing the casting volume.[25] (b) The honeycomb-patterned film is transferred onto a glass substrate with an ethanol-soluble sacrificial coating of poly(styrene-*co*-allyl alcohol) (Mw: 2,200, Aldrich), which has been spin-coated using an ethanol solution of ~1 wt%. The honeycomb-patterned film is placed with the original top surface (with circular holes) facing the sacrificial coating. (c) Next, the half layer of the honeycomb-patterned film is peeled off with a sheet of adhesive tape (Scotch Tape, 3M, Japan), resulting in a porous film with "pillars".[24] (d) The porous film is dethatched from the glass substrate in an ethanol bath, in which the sacrificial layer of poly(styrene-*co*-allyl alcohol) is dissolved. (e) Then, the porous film is transferred to another glass slide with the side of the "pillars" facing the glass slide and dried. (f) Schematic of the porous film with "pillars" placed on a glass slide, which is to be embedded at the surface of a thermally-curable elastomer (Fig. 1).

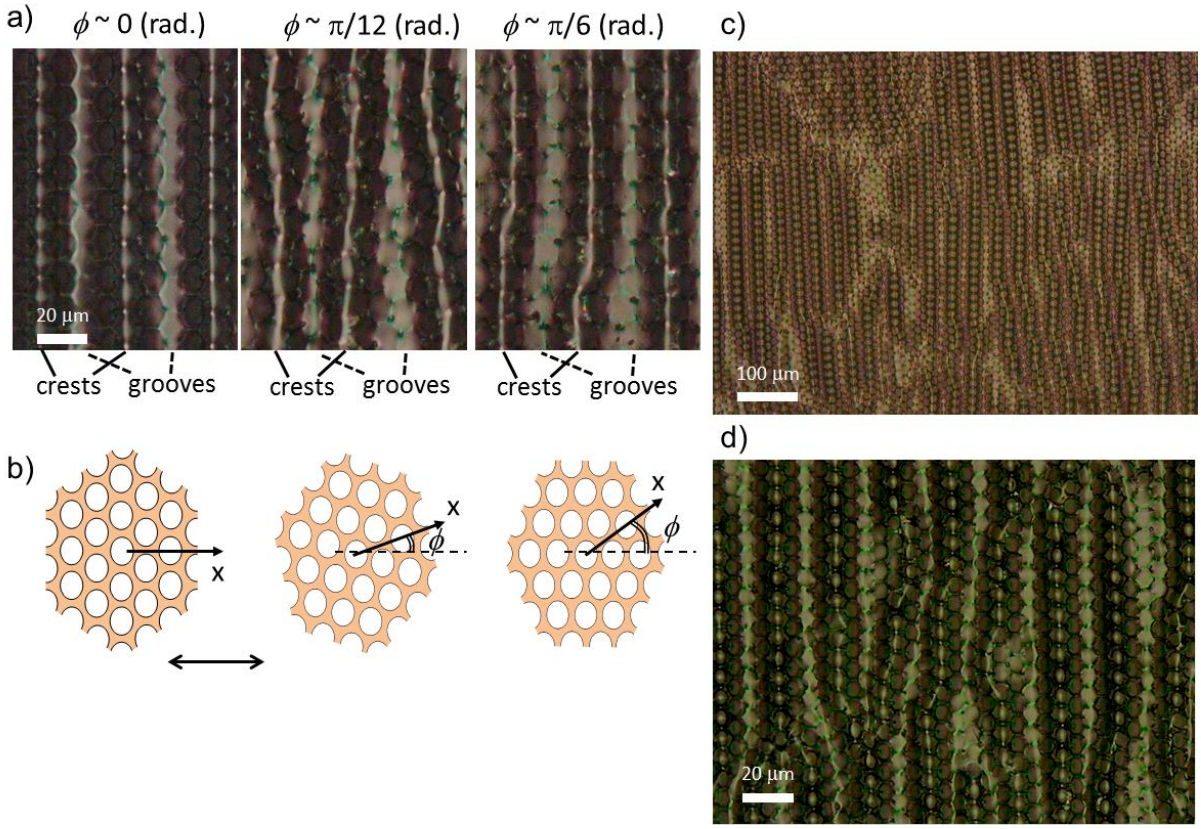

Figure S2. Effect of the relative angle ϕ between the axis of compression and that (x axis) attached to the hexagonal lattice of the embedded porous film on the wrinkle patterns at s = 0.1. (a) Optical microscope images of representative wrinkle patterns and (b) the corresponding schematics of the configurations of embedded hexagonal lattices at different values of ϕ. At $\phi \sim 0$, the regular wrinkles with the wavelength $\lambda = 4(3^{1/2}/2)\Lambda(1\text{-}s)$ mainly appear, where $\Lambda \sim$ 11 μm. For $0 < \phi < \pi/12$, the crest lines are irregularly zigzagged. At $\phi \sim \pi/6$, the wrinkles of $\lambda = 3\Lambda \sim 4\Lambda$ formed with the regularity less than that at $\phi \sim 0$. Though admittedly crude, the averaged wrinkle wavelength λ_{av} ~34 μm at s = 0.1 independent of ϕ. Also independent of ϕ, the crests and the grooves are located at the beams of the porous film, at which the bending rigidity is expected to be lower than the other parts of the porous framework. (c) An optical image showing a larger area. All the wrinkle patterns shown in (a) can be found. Note that the wrinkle formation is sometimes suppressed at the domain boundaries of the hexagonal lattice. This might be due to the locally-increased bending rigidity of the porous film at the domain boundaries, at which the width (and thickness) of the beam between holes is increased by the loose packing of holes. (d) An optical image for wrinkled surface using a porous film with smaller $\Lambda \sim 7$ μm. Note that the size of the scale bar is identical to that in (a). The wrinkle wavelength is approximately 22 μm, which also roughly corresponds to the relationship $\lambda = 4(3^{1/2}/2)\Lambda(1\text{-}s)$. The periodicity of the porous film was controlled by changing the casting volume when the original honeycomb film was fabricated[25].

Supplementary Information 2. **Discussion on increased bending rigidity of porous film**.

It is clear from the structure of the present porous film that the position with the lowest local bending rigidity is in the middle of the beam with the cross section of a quasi-triangular shape. Indeed, the crests and the grooves of the resultant wrinkles, at which the highest curvature appear, correspond in position to the middle of the beams particularly for the case with $\phi \sim 0$. Therefore, here we discuss the bending rigidity of the part (beam) with a simplified model, a triangular-beams model, shown in a schematic below.

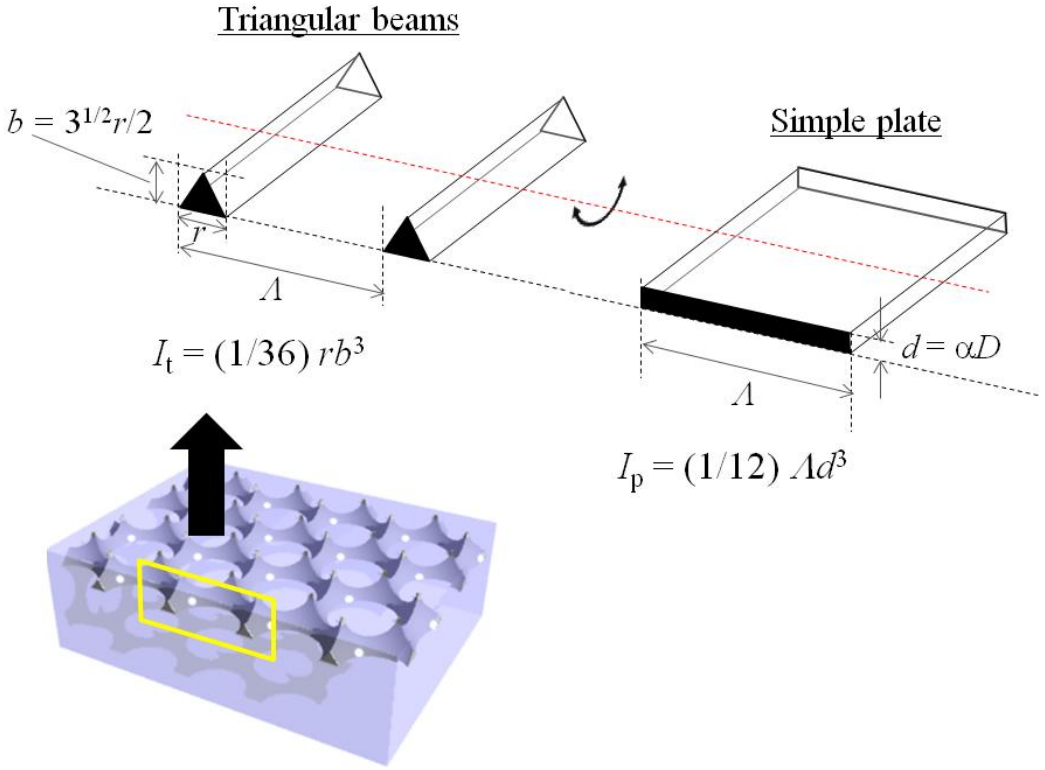

The part of interest is composed of beams with the cross section of an equilateral triangle (the side length is r), which align in parallel with a distance of Λ. The second moment of area per length Λ for the triangular beams is expressed as $I_t/\Lambda = (1/36)\, rb^3/\Lambda = (3^{1/2}/96)r^4/\Lambda$. (Here, for simplicity, we consider the bending rigidity neglecting deformation expressed by the Poisson's ratio.) Meanwhile, the second moment of area per length Λ for the simple "plane" plate, which has an identical mass per unit area to that of the present porous film, is expressed as $I_p/\Lambda = (1/12)d^3 = (1/12)(\alpha D)^3$. For materials with the identical Young's modulus, the bending rigidity is simply proportional to the second moment of area. Thus, the ratio of the bending rigidity of the triangular beams to that of the simple "plane" plate, $R = I_t / I_p = [(3^{1/2})/8][r^4/(\Lambda[\alpha D]^3)]$. Using the experimental values; $r \sim 2.5$ μm, $\Lambda \sim 10$ μm, $D \sim 3.5$ μm, and $\alpha = 0.1$~0.2, R can be calculated as 2.2~17.9 (>1). This indicates that even the part with the lowest bending rigidity in the porous film has the higher bending rigidity than that of the corresponding "plane" plate. The actual structure of the present porous film is further more complex than that of the present model and it is also supported by (embedded in) a soft elastic substrate. Thus, more rigorous treatment would be required for detailed discussions. Nevertheless, this simple discussion qualitatively supports the increased bending rigidity of the present porous film by the geometrical factor (the structure of the triangular beam).

Supplementary Information 3. Simulation details.

In the simulation, we modeled the system by an elastic membrane with non-uniform (effective) bending rigidity and supported by a soft substrate. The local bending rigidity is largest and smallest at pillars and holes, respectively, and takes intermediate values at beams. The role of the substrate is represented by Hookean springs vertically bonding the membrane and the bottom plane. Assuming small deformations, we employed the Föppl-von-Kármán approximation in which the strain tensor is written in terms of the displacement field $u(x,y)$ as

$$e_{ij} = \frac{1}{2}\left[\frac{\partial u_i}{\partial r_j} + \frac{\partial u_j}{\partial r_i} + \left(\frac{\partial u_z}{\partial r_i}\right)\left(\frac{\partial u_z}{\partial r_j}\right)\right].$$

The total elastic energy reads

$$E = \frac{1}{2}\iint dxdy\left[h\lambda_e e_{ii}^2 + 2h\mu_e e_{ij}^2 + \kappa(\nabla^2 u_z)^2 + \nu u_z^2\right],$$

where $h=h(x,y)$ is the effective thickness of the membrane, λ_e and μ_e are the Lame moduli, $\kappa = \kappa(x, y) \propto h(x,y)^3$ is the local bending rigidity and ν is the spring constant for the vertical bonds. The displacement obeys
the relaxational dynamical equation

$$\frac{\partial u_i}{\partial t} = -\Gamma\frac{\delta E}{\delta u_i}$$

to locally minimize the total energy. We discretized the model on a triangular lattice and assume the spatial distribution of bending rigidity as schematized below.

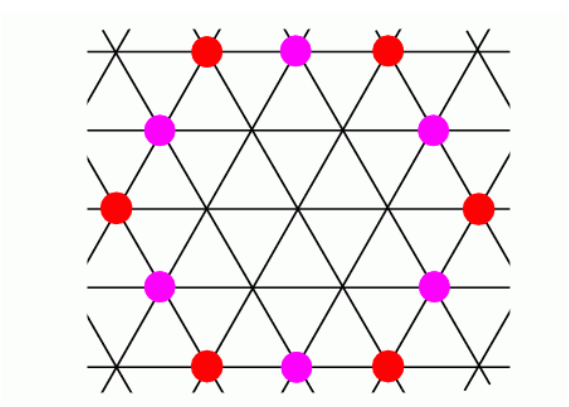

At the red and pink points, which correspond to pillars and beams, respectively, the membrane has 10 and 5 times larger effective thickness than at the other points, which correspond to holes. Assuming periodic boundary condition on a rhombic area with 96^2 lattice points, we imposed a 5% horizontal strain on the membrane. For the initial condition we used a small-amplitude sinusoidal profile with a prescribed period and phase, and examined the stability of the pattern in the course of time-evolution. As shown in Fig. 2h, we find that the wave pattern with the crests and grooves lying on the beams, which is similar to the one observed in the experiment, remains stable. The average depth of the wrinkle in the final stage of the simulation was 8.1% of the period.

Note that in the present simple model the detailed three-dimensional structure of the porous film is not directly treated but indirectly expressed by the periodic modulation of the local thickness h of the plane film. For rigorous discussion, the relationship between the detailed structure and h should be clarified, which may be possible by comparing the results with the more accurate simulations and remains to be tackled. However, results of the present simple model are sufficient for the confirmation of validity of the geometrical coupling between the wrinkle wave and the underlying periodic patterns.

Caption for **Supplementary Information Movie 1**.

This movie shows scratching tests under the optical microscope. Firstly, the normal wrinkles of a polystyrene film supported by a PDMS substrate under a uniaxial compressive strain of ~0.15 are scratched manually using a needle. The film suffers delamination and breaks, which are fatal damages for wrinkling. In contrast, present reinforced wrinkles show no damage during and after the scratching tests.